Translational Fidelity Mutations in 18S rRNA Affect the Catalytic Activity of Ribosomes and the Oxidative Balance of Yeast Cells†

Theodoros C. Konstantinidis,‡ Nikolaos Patsoukis,§ Christos D. Georgiou,§ and Dennis Synetos*,‡

Laboratory of Biochemistry, School of Medicine, and Department of Biology, University of Patras, 261 10 Patras, Greece

Received December 8, 2005; Revised Manuscript Received February 6, 2006

ABSTRACT: The function of mutations *rdn1A*, *rdn1T*, and *rdn2* in 18S rRNA of *Saccharomyces cerevisiae* is investigated. The mutations correspond to substitutions C1054A, C1054U in helix 34, and G517A in helix 18 of 16S rRNA in *Escherichia coli*, respectively, in which the first and third mutations caused nonsense suppression, while C1054U caused no suppression. In yeast, *rdn1A* caused phenotypic suppression at nonsense codons, whereas *rdn1T* and *rdn2* caused antisuppression. We provide in vitro evidence that, in addition, *rdn1A* decreases translational accuracy at sense codons as well, by a factor of 8, accompanied by extreme sensitivity to paromomycin, compatible with its error-prone character. Mutations *rdn1T* and *rdn2* exhibit hyperaccuracy and paromomycin resistance. Thus, mutations in conserved rRNA regions may affect the same functions in the various species but in opposite directions. Mutation *rdn1A*, but not *rdn1T* or *rdn2*, affected also the catalytic activity of the ribosome, a 60S subunit activity. The rate of peptide bond formation was reduced to half its normal value, indicating a communication between the two subunits. Moreover, error-prone mutation *rdn1A* was less susceptible to oxidative modifications than wild type, indicated by decreased lipid peroxidation and nonprotein/protein disulfides, as well as by increased protein thiols. In contrast, hyperaccurate mutations *rdn1T* and *rdn2* displayed increased oxidative stress. Our results suggest that the cells may consume more energy to achieve hyperaccuracy leading to increased oxidative modifications.

The ribosome is a subcellular organelle responsible for the accurate decoding of the genetic information carried in mRNA and for protein synthesis via peptide bond formation. The first process takes place in the decoding center, which is assembled by nucleotides from helices 18, 24, 27, 34, and 44 of 16S (18S) ribosomal RNA (*1*) and some ribosomal proteins (*2*). Peptide bond formation is carried out in the peptidyltransferase center, which is apparently composed mainly from nucleotides of domain V of 23S (25S) rRNA (*3*, *4*).

The 18S rRNA of yeast is 256 nucleotides longer than the 16S rRNA of *Escherichia coli*, but its overall tertiary structure is well conserved (*5*). Helix 44 of 18S rRNA is the conserved core of the decoding region. Two of its universally conserved bases, A1492 and A1493, are essential for cell viability and for A-site tRNA binding (*6*). In the presence of mRNA and cognate tRNA in the ribosomal A-site, A1492 and A1493 flip out of the interior of helix 44 and interact with the second and first base pairs of the codon−anticodon helix, respectively (*7*). In this way, they cause transition of the small ribosomal subunit from an open to a closed conformation, making the recognition of cognate aminoacyl-tRNA more favorable than that of near-cognate aminoacyl-tRNA (*8*). Furthermore, this long helix of the small subunit is involved in several of the contacts between the two ribosomal subunits, e.g. with 5.8/25S rRNA or with ribosomal proteins rpl23 and rpl24 of the large subunit (*5*). Helix 27 of the 16S (18S) rRNA contacts helix 44 below the decoding region (*9*), and it is also involved in a bridge to the 5.8/25S rRNA of the large subunit of yeast (*5*). Moreover, in *E. coli*, the 900 tetraloop that caps helix 27 of 16S rRNA forms a motif that docks into the minor groove of three base pairs at the bottom of helix 24 of 16S rRNA (*10*). Both the tetraloop and its receptor in helix 24 contact helix 67 of 23S rRNA, forming the B2c intersubunit bridge (*11*). Mutations in helix 24 and/or helix 27 have an impact on translational fidelity due to a possible perturbation of B2c assembly or structure (*10*).

Nucleotides from helix 18 and helix 34 of 16S rRNA also participate in the assembly of the decoding site. It has been found that G530 of helix 18 undergoes a conformational change in the presence of mRNA and aminoacyl-tRNA and interacts with A1492 in helix 44, with the anticodon in the second position and with the codon in the third position, whereas C1054 of helix 34 stacks against G36 of the anticodon stem loop of A-site-bound tRNA (*7*). Moreover, mutations in the 530 loop of helix 18, in helix 34, and in the 1400−1500 region of helix 44 of 16S rRNA distort the site of codon−anticodon interaction, leading to impaired discrimination between cognate and near-cognate aminoacyl-tRNAs at both A and P ribosomal sites (*12*). Recent kinetic

† This work was supported by the European Social Fund (EKT), the Operational Programme for Educational and Vocational Training II (EPEAEK II), and particularly the Programme HERAKLEITOS.

* To whom correspondence should be addressed. Tel: +30 2610 996125. Fax: +30 2610 997690. E-mail: dsynetos@med.upatras.gr.

‡ Laboratory of Biochemistry, School of Medicine, University of Patras.

§ Department of Biology, University of Patras.

10.1021/bi052505d CCC: $33.50
Published on Web 02/28/2006

studies have shown that efficient tRNA discrimination is based on the large differences in the forward reaction rates of GTPase activation and accommodation (*13*).

Increasing evidence suggests the existence of an intimate cross talk between the two ribosomal subunits and that an element of one subunit affecting a specific activity of this subunit may have pleiotropic effects on functions of the other. Thus, mutations in the large subunit, e.g., *rdn5* in the sarcin/ricin loop of yeast 25S rRNA (*14*), or in ribosomal proteins, e.g., in L39 (*15*), not only influence the 60S subunit-associated catalytic activity of the ribosome but also affect translational fidelity, a 40S subunit-associated activity.

In yeast, mutation *rdn1A* (C1054A, *E. coli* nomenclature) in helix 34 of 18S rRNA was found to cause dominant nonsense suppression, whereas mutation *rdn1T* (C1054U) was a recessive antisuppressor (*16*). Yeast *rdn2* (G517A) in helix 18 of 18S rRNA was shown to inhibit nonsense suppression induced by paromomycin (*17*). Of the corresponding substitutions in *E. coli*, C1054A and G517A behave as translational suppressors and reduce translational fidelity, while C1054U does not affect fidelity (*18*, *19*).

In the present work, we examined whether mutations *rdn1A*, *rdn1T*, and *rdn2*, apart from affecting readthrough at stop codons, affected also the accuracy of decoding at sense codons as well. Moreover, we examined their influence on other parameters of protein synthesis including peptidyltransferase activity. We found that a translational fidelity mutation belonging to the 40S subunit may affect the catalytic activity, a 60S subunit activity, lending further support to the notion that the two subunits intercommunicate.

Translational fidelity and oxidative balance are two of several parameters affected during cell aging. The production of free radicals during metabolic processes enhances the oxidative modification of protein targets including translational elongation factors (*20*). Studies conducted in prokaryotes have demonstrated that increased levels of transcriptional and translational errors induce protein oxidation (*21*). Thus, the possible effect of translational fidelity mutations on the oxidative status of the yeast cell was also targeted in this study.

MATERIALS AND METHODS

Strains and Plasmids. The previously constructed strains *rdnwt* (L1494), *rdn1A* (L1583), *rdn1T* (L1597), and *rdn2* (L1522) (*16*, *17*) were used in the present study. All strains contain complete and stable deletions of the chromosomal 9 kb rDNA units (*RDN*) and a new multicopy plasmid pRDN carrying in tandem the genes for 18S, 25S, 5.8S, and 5S rRNAs as well as regulatory sequences. Moreover, strains L1583, L1597, and L1522 carry in addition substitutions C1054A (*rdn1A*), C1054U (*rdn1T*) in helix 34, and G517A (*rdn2*) in helix 18 of 18S rRNA (Figure 1 and Table 1), respectively. All substitutions were introduced to and expressed through the high-copy plasmid pRDN.

In Vivo Procedures. Cells from the various strains were grown in YPD medium containing 1% yeast extract, 2% peptone, and 2% D-glucose at 30 °C.

To measure sensitivity of the various strains toward selected antibiotics, such as paromomycin, 10^5 cells/mL from each freshly grown yeast colony were added to YPD media containing increasing concentrations of paromomycin. Cells were grown at 30 °C until the culture without antibiotic was grown to an optical density at 660 nm of 0.9, which was taken as 100%. At this point, growth of all cultures was stopped. Increasing concentrations of the drug begin to inhibit cell growth, resulting in optical density decreases. For each strain, the concentration of paromomycin required for 50% inhibition of cell growth was determined.

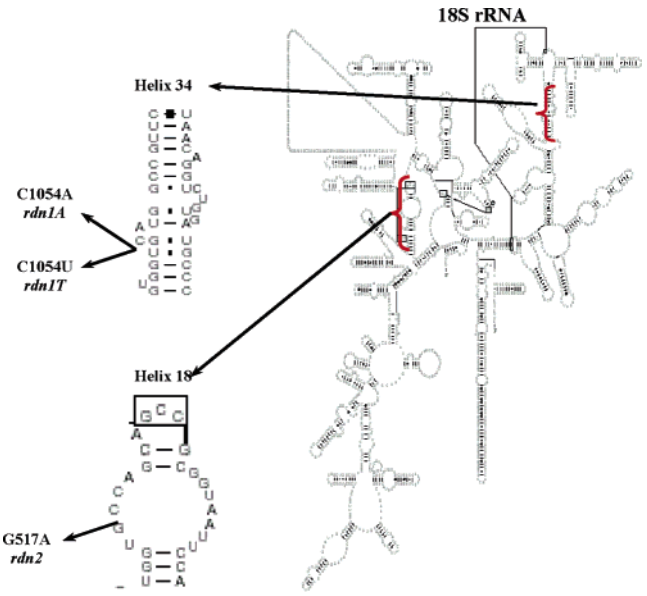

FIGURE 1: Secondary structure of the *S. cerevisiae* 18S rRNA (related information is available at http://www.rna.icmb.utexas.edu). The positions of mutations *rdn1A*, *rdn1T* in helix 34, and *rdn2* in helix 18, corresponding to nucleotide substitutions C1054A, C1054U, and G517A, respectively, are indicated.

Alternatively, the sensitivity toward antibiotics was determined with the antibiotic disk assay, in which approximately 10^7 cells were spread evenly on YPD plates containing in addition 2% agar. Paromomycin at the appropriate concentrations was pipetted onto 5 mm Whatman (3MM) paper disks placed evenly on the surface of the YPD medium. The plates were incubated at 30 °C for 3−6 days. Clear and white circles around the disks indicate sensitivity and phenotypic suppression, respectively.

In Vitro Procedures. The preparation of a yeast cell-free system, the translation of poly(U) templates, the fidelity of translation expressed as the error frequency measured by the misincorporation of [^{3}H]leucine, the time course of polyphenylalanine synthesis using [^{3}H]Phe-tRNA, the A- and P-site binding studies, and the sucrose gradient analysis were all carried out as described previously (*15*).

Preparation of a Ternary Complex Active in Peptide Bond Formation. Unwashed ribosomes and soluble protein factors from wild-type or mutant yeast cells as well as Ac-[^{3}H]Phe-tRNA were prepared as described recently (*14*). Complex C, i.e., the Ac-[^{3}H]Phe-tRNA·poly(U)·80S ribosome complex, was formed and purified through adsorption on cellulose nitrate filter disks. The filter disks with the adsorbed complex C were gently shaken for 45 min at 5 °C in binding buffer containing 0.05% Zwittergent 3-12 (ZW) (1.8 mL/whole disk). The extraction was stopped by removing the filters, and the complex C-containing ZW extract was used in the puromycin reaction. The amount of Ac-[^{3}H]Phe-tRNA bound to poly(U)-programmed ribosomes was determined

Table 1: Genotypes of Yeast Strains

strain	genotype	mutation
wt (L1489)	*MAT*α *ade1−14*(UGA) *his7−1*(UAA) *leu2−3,112 lys2-L864*(UAG) *trp1*Δ*1 ura3−52*	none
rdnwt (L1494)	*MAT*α *ade1−14*(UGA) *his7−1*(UAA) *lys2-L864*(UAG) *leu2−3,112 trp1*Δ*1 ura3−52RDN*Δ pRDN-wt (*TRP1 LEU*2-d rDNA)	none
rdn1A (L1583)	*MAT*α *ade1−14*(UGA) *his7−1*(UAA) *lys2-L864*(UAG) *leu2−3,112 trp1*Δ*1 ura3−52RDN*Δ pRDN-1A (*TRP1 LEU*2-d rDNA)	C1054A
rdn1T (L1597)	*MAT*α *ade1−14*(UGA) *his7−1*(UAA) *lys2-L864*(UAG) *leu2−3,112 trp1*Δ*1 ura3−52RDN*Δ pRDN-1T (*TRP1 LEU*2-d rDNA)	C1054U
rdn2 (L1522)	*MAT*α *ade1−14*(UGA) *his7−1*(UAA) *lys2-L864*(UAG) *leu2−3,112 trp1*Δ*1 ura3−52RDN*Δ pRDN-2 (*URA3* rDNA)	G517A

by measuring the trapped radioactivity in the ZW extract in a scintillation spectrometer.

In Vitro Assay for Peptidyltransferase Activity. The reaction between the Ac-[^{3}H]Phe-tRNA of complex C in the ZW extract and puromycin (puromycin reaction) was carried out as described recently (*14*). ZW extract (0.9 mL) was preincubated for 2 min at 30 °C and then reacted with puromycin. At the end of each incubation period, the percentage (x) of the bound donor, Ac-[^{3}H]Phe-tRNA, that was converted to product P (Ac-[^{3}H]Phe-puromycin) was measured. Each percentage (x) was corrected by dividing its value, first, with factor A ($A = C/C_0$, where C and C_0 are the amounts of surviving complex C in binding buffer at the end of each incubation period and at zero time, respectively), and, second, with the extent factor α. The extent factor is determined when complex C is allowed to react completely at any concentration of puromycin. By the first correction (x/A), the parallel inactivation of complex C during the puromycin reaction is subtracted, while by the second correction, the intervention of any species other than complex C is erased as if 100% of the bound Ac-[^{3}H]Phe-tRNA were reactive toward puromycin. Thus, the experimental values of x were corrected by factor $A\alpha$, i.e., $x' = x/A\alpha$.

Preparation of Cells and in Vitro Assays for the Study of Oxidative Stress. Yeast cells were grown in YPD medium at 30 °C up to 10^8 cells/mL, diluted in the appropriate buffer, lysed with glass beads, and centrifuged at 4000*g* for 5 min at 4 °C. The supernatant was collected and used for the determination of lipid peroxidation and nonprotein disulfides (NPSSR). Lipid peroxidation was assayed by a modified thiobarbituric acid- (TBA-) based method (*22*). Specifically, 0.35 mL of the sample was mixed with 0.35 mL of TBA reagent followed by addition of 5 μL of a 2% (w/v) solution of the lipid antioxidant butyl hydroxyanisole. The mixture was incubated at 100 °C for 20 min and brought to room temperature, then 0.7 mL of 1-butanol was added, and the mixture was centrifuged at 15000*g* for 3 min. Absorbance of the upper butanol layer was measured at 535 and 600 nm against appropriate sample and reagent blanks. The absorbance difference between 535 and 600 nm was converted to malondialdehyde (MDA) equivalents using the extinction coefficient for MDA, 1.55×10^5 M^{-1} cm^{-1} (*22*). Lipid peroxidation was expressed in picomoles of MDA equivalents per milligram of total protein.

Nonprotein disulfides (NPSSR), isolated by fractional trichloroacetic acid- (TCA-) based protein precipitation, were determined in the resulting supernatant by a photometric method based on the reaction of Ellman's reagent 5,5′-dithiobis(2-nitrobenzoic acid) (DTNB) with thiol sulfhydryl groups after reduction of nonprotein disulfide bridges by borohydride (BH) (*22*). In addition, protein thiols (PSH) and protein disulfides (PSSP) were determined in the resulting protein pellet by the same photometric method, according to which the protein pellet was urea-solubilized to expose PSH thiol groups to DTNB as well as those resulting from PSSP after BH reduction.

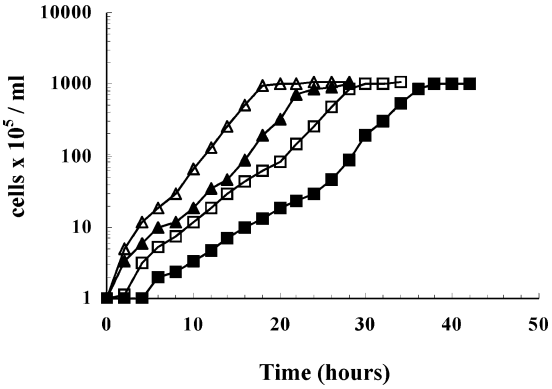

FIGURE 2: Growth curves of wild-type and *rdn* mutant strains. Cells, 10^5/mL of each culture, were added to YPD medium and grown at 30 °C. The number of cells was monitored in a hemocytometer at appropriate time intervals. The curves represent growth of the following strains: *rdnwt* (open triangles), *rdn1A* (solid squares), *rdn1T* (solid triangles), and *rdn2* (open squares).

Statistical Analysis. The data variability was estimated using the one-way analysis of variance (ANOVA) procedure. We used the F-Scheffè test to determine which means were significantly different from each other. All statistical tests were performed using an SPSS program for MS Windows, release 6.0.

RESULTS

Growth Rates of rdn Mutant Strains. The introduction of high-copy plasmid pRDN (strain L1494, Table 1) was not entirely innocuous for the cell. This strain, *rdnwt*, grew with a doubling time of 118 min compared to 96 min for the wild-type strain carrying the chromosomal RDN locus (strain L1489). Impressively, nucleotide substitutions at a position of 18S rRNA corresponding to C1054 of *E. coli* 16S rRNA led to widely different growth rates. Thus, cells carrying adenine in place of cytosine (*rdn1A*) caused a very poor growth phenotype; their doubling time was increased to 280 min (Figure 2). In contrast, cells carrying uracil in place of cytosine (*rdn1T*) grew with a doubling time of only 154 min, i.e., at a rate twice as fast as that of *rdn1A* and only slightly slower than *rdnwt*. The third mutant, *rdn2* (G517A), in agreement with previous findings (*17*), exhibited also a slow growth phenotype and grew with a doubling time of 200 min.

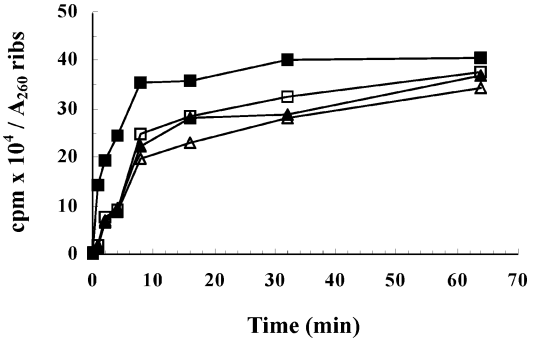

FIGURE 3: Time courses of polyphenylalanine synthesis. Poly(U)-programmed wild-type and *rdn* mutant ribosomes were incubated with [^{3}H]Phe-tRNA at 30 °C for the indicated time intervals. The curves correspond to the following strains: *rdnwt* (open triangles), *rdn1A* (solid squares), *rdn1T* (solid triangles), and *rdn2* (open squares).

Table 2: Translational Error Frequencies (EF) in Vitro of Wild-Type and Mutant Ribosomes in the Absence or Presence of 50 μM Paromomycin (PM)

	EF ± SE	
strain	−PM	+50 μM PM
rdnwt	0.0040 ± 0.0008	0.0893 ± 0.0093
rdn1A	0.0309 ± 0.0017[a]	0.3711 ± 0.0221[b]
rdn1T	0.0027 ± 0.0007	0.0136 ± 0.0015[b]
rdn2	~0[a]	0.0052 ± 0.0008[b]

[a] Statistically different (one-way analysis of variance, F-Scheffè test, $p < 0.05$) from the wild type in the absence of PM. [b] Statistically different (one-way analysis of variance, F-Scheffè test, $p < 0.05$) from the wild type in the presence of 50 μM PM.

Polyphenylalanine Synthesis Capacity of rdnwt and rdn Mutant Ribosomes. The protein synthesis activity of wild-type and mutant yeast ribosomes was measured in vitro from the rate and extent of polyphenylalanine synthesis in a poly-(U)-dependent translation system.

In this system, the rate of protein synthesis of the *rdn1A* ribosomes was twice as high as the wild-type and the other strains under study, indicated by the steeper slope of the curve (Figure 3). Apparently, *rdn1A* ribosomes recognize the codon triplet (UUU) in a more efficient and rapid way than the other strains. All other strains, including the wild type, exhibited similar initial rates of polyphenylalanine synthesis. As expected, the *rdn1A* ribosomes reached maximal phenylalanine incorporation earlier than the other strains, i.e., after 8 min compared to at least 32 min for the other strains. Nevertheless, the extent of the reaction, corresponding to the total amount of polyphenylalanine formed, was similar for all strains.

Effect of 18S rRNA Mutations on Translational Fidelity in Vitro. It has been previously shown in yeast that mutation *rdn1A* caused suppression and increased readthrough at stop codons whereas mutations *rdn1T* and *rdn2* caused antisuppression and reduced readthrough at stop codons. To examine whether these mutations affect the accuracy of decoding at sense codons as well, we measured the misincorporation of the near-cognate amino acid leucine relative to the cognate amino acid phenylalanine using a poly(U)-dependent cell-free translation system.

As shown in Table 2, *rdn1A* ribosomes exhibited decreased translational fidelity by a factor of 8; the error frequency was raised from 0.0040 for the wild type to 0.0309, i.e., from 40 to 309 misincorporated leucines per 10000 translated codons. In contrast, *rdn1T* ribosomes improved the translational fidelity levels, as shown by the reduction of the error frequency from 0.0040 to 0.0027. Finally, *rdn2* ribosomes increased translational fidelity, to such a degree that the error frequency was nearly zero; i.e., no leucine misincorporation was observed in our in vitro system. On the strength of these in vitro results, mutation *rdn2* is the most hyperaccurate mutation identified to date.

Ribosomal RNA is a target for several antibiotics (*23*). Aminoglycoside antibiotics bind to the decoding center of yeast ribosomes, making the protein-synthesizing machine more susceptible to errors during translation (*16*). Paromomycin is such an antibiotic; it binds in the interior of helix 44 (*7*) and causes misreading by inducing increased binding of near-cognate aminoacyl-tRNA to the A-site of the ribosome (*24*). In agreement with this, paromomycin at 50 μM caused a general increase of the error frequencies in all strains, confirming its character as an error-inducing agent. The error frequency of the wild type itself was raised substantially by 853 additional misincorporations per 10000 translated codons (Table 2). However, the increase was highest for *rdn1A* ribosomes in which the error frequency was raised by 3432 additional misincorporations per 10000 translated codons. Interestingly, strains *rdn1T* and, especially, *rdn2* confirmed their own error-restrictive character since in the presence of paromomycin their error frequencies were slightly raised but remained below wild-type levels of increase; i.e., they were raised by only 109 and 52 misincorporations per 10000 translated codons, respectively.

The results reported here were obtained with 11 mM Mg^{2+} in the in vitro translation assays. Similar results were subsequently obtained at conditions closer to the in vivo situation, i.e., at 2.5 mM Mg^{2+} and 3 mM spermidine.

Paromomycin Sensitivity and Suppression Associated with 18S rRNA Mutations. The loss of translational accuracy caused by paromomycin has often been linked to hypersensitivity of the mutant strains toward this antibiotic. Figure 4A shows that the growth of the *rdn1A* strain was inhibited by 50% at 16 μM paromomycin compared to 47 μM for the *rdnwt* strain. Conversely, 50% inhibition of cell growth was increased slightly to 57 μM paromomycin for the slightly hyperaccurate *rdn1T* strain and to as much as 508 μM paromomycin for the highly hyperaccurate *rdn2* strain.

These findings were further supported with the antibiotic disk assay, the results of which are depicted in Figure 4B. This method determines levels of suppression as well as paromomycin sensitivity. The white color of the *rdn1A* cells on YPD medium indicates strong suppression of the *ade1−14* (UGA) marker while the light red color of the *rdn1T* cells indicates antisuppression and the dark red color of *rdn2* cells indicates even stronger antisuppression of the *ade1−14* (UGA) marker.

A further finding of this assay was the determination of paromomycin sensitivity associated with the three mutants under study. By comparing antibiotic-induced zones of growth inhibition (Figure 4B), we observed that *rdn1A* cells are more sensitive to paromomycin than *rdnwt* cells, since in a 9 cm diameter YPD plate the *rdn1A* cells had an area of growth inhibition (clear circles), in which the distance of the cells from the disk soaked with 5 μL of 1000 mg/mL paromomycin was 14 mm compared with 6 mm for the

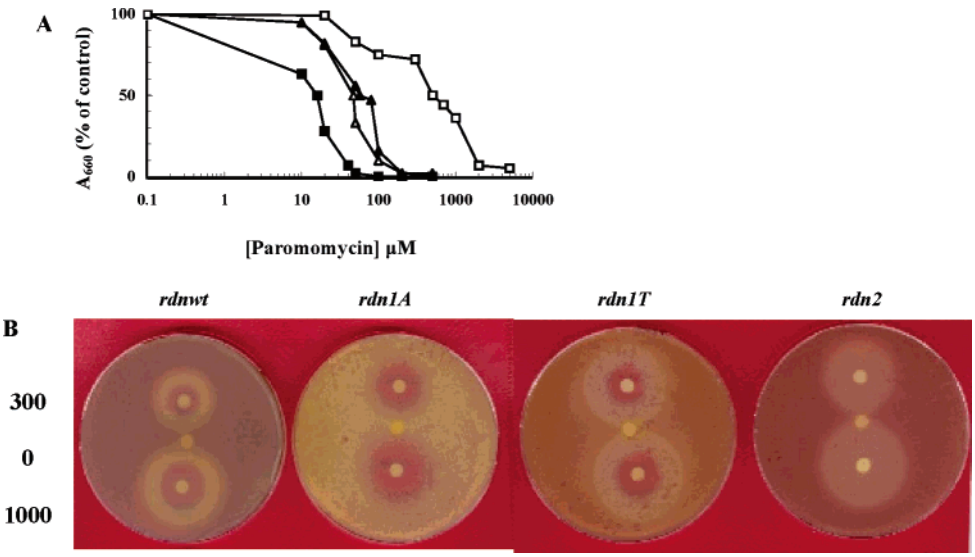

FIGURE 4: Inhibition of cell growth in the presence of paromomycin. (A) Cells were grown in YPD at 30 °C until the culture without antibiotic reached an A_{660} of 0.9, which was taken as 100%. Concentrations of paromomycin are as indicated. The curves correspond to the following strains: *rdnwt* (open triangles), *rdn1A* (solid squares), *rdn1T* (solid triangles), and *rdn2* (open squares). (B) Antibiotic activity disk assay. Cells (~10^7) from *rdnwt* or mutant strains were spread on YPD plates and grown at 30 °C. Paromomycin at the indicated concentrations (300 and 1000 mg/mL) or water as control (5 μL) was pipetted onto filter paper disks. Clear circles around the disks indicate the killing effect of the antibiotic. Red or white colonies indicate phenotypic antisuppression or suppression, respectively, of the genetic marker *ade1−14*(UGA). From left to right: *rdnwt* strain, *rdn1A* strain, *rdn1T* strain, and *rdn2* strain.

Table 3: Effect of *rdn* Mutations on the Binding of Phe-tRNA and Ac-Phe-tRNA to A- and P-Sites and on the Peptidyltransferase Activity of Yeast Ribosomes

	% of control		k_3	K_s	k_3/K_s
strain	A-site	P-site	(min^{-1})	(mM)	(min^{-1} mM^{-1})
rdnwt	100[a]	100[b]	1.46 ± 0.04	0.85	1.72
rdn1A	175 ± 14[c]	105 ± 5	0.82 ± 0.07[c]	0.79	1.04
rdn1T	87 ± 8	97 ± 9	1.32 ± 0.08	0.80	1.65
rdn2	86 ± 7	99 ± 7	1.25 ± 0.06	0.75	1.67

[a] 100% represents 0.162 molecule of [^{3}H]Phe-tRNA bound to the A-site per molecule of ribosomes. [b] 100% represents 0.106 molecule of Ac-[^{3}H]Phe-tRNA bound to the P-site per molecule of ribosomes. [c] Statistically different (one-way analysis of variance, F-Scheffè test, $p < 0.05$) from the wild type.

isogenic *rdnwt* cells. In contrast, *rdn1T* cells are slightly more resistant to paromomycin than *rdnwt* cells, while *rdn2* cells are a lot more resistant than *rdnwt* cells. Under the conditions described above, the relative distances were 5 and 0 mm, respectively. It should be noted that the white circles around the disks are indicative of a level of suppression caused by paromomycin in analogy to the increased error frequencies caused by paromomycin in vitro.

These results indicate that in the case of the *rdn1* and *rdn2* mutations the misreading and killing effects of paromomycin operate in concert. This is not always the case; e.g., in *rdn5*, a mutation of 25S rRNA recently studied (*14*, *25*), the two effects were separate.

Effect of rdn Mutations on the Binding of [^{3}H]Phe-tRNA and Ac-[^{3}H]Phe-tRNA to Ribosomal A- and P-Sites, Respectively. Table 3 shows the A-site binding capacities of the *rdn* mutant strains for the cognate aminoacyl-tRNA expressed as percent of the radioactivity contained in the Phe-tRNA·80S·poly(U) complex. Of the three *rdn* mutants under consideration, only *rdn1A* showed a substantial increase, i.e., 75%, in its ability to bind Phe-tRNA compared to wild type. Such increased stability of aminoacyl-tRNA binding has also been observed for other error-prone mutations (*14*, *15*). The other two strains, *rdn1T* and *rdn2*, displayed a slightly decreased A-site binding of cognate aminoacyl-tRNA. Such decreased stability has also been found for other error-restrictive mutations (*26*).

Our results on P-site binding (Table 3) show that none of the mutations under study affected significantly the Ac-[^{3}H]-Phe-tRNA binding, an indication that none of the two nucleotides, C1054 or G517, is placed close enough to the ribosomal P-site.

Effect of rdn Mutations on Peptide Bond Formation. Ternary complex C, prepared as described in Materials and Methods, contained 27% of the input Ac-Phe-tRNA (3.2 A_{260} units or 42 pmol of Ac-Phe-tRNA/0.2 mL of binding mixture), since only 27% of the input of the radioactivity was adsorbed on the cellulose nitrate filter disk. Thus, complex C contained 11.3 pmol of Ac-Phe-tRNA. Assuming a 1:1 combination, this complex C also engages 10.6% of the ribosomes added (6.0 A_{260} units or 107.3 pmol). Hence, 0.106 molecule of Ac-Phe-tRNA is bound per molecule of poly(U)-programmed ribosomes.

The peptidyltransferase activity of ribosomes was assessed by the puromycin reaction carried out at 30 °C in the presence of 9 mM Mg^{2+}. Under these conditions, the reaction between complex C and excess puromycin (S) follows pseudo-first-order kinetics to produce Ac-Phe-puromycin (P):

$$C + S \overset{K_s}{\rightleftharpoons} CS \overset{k_3}{\rightleftharpoons} C' + P \quad (1)$$

At each concentration of puromycin, the apparent first-order rate constant k_{obs} can be calculated from semilogarithmic time plots, represented by the relationship

$$k_{obs} = k_3[S]/(K_s + [S]) \quad (2)$$

where k_3 is the catalytic rate constant and K_s is the dissociation constant of the encounter complex CS.

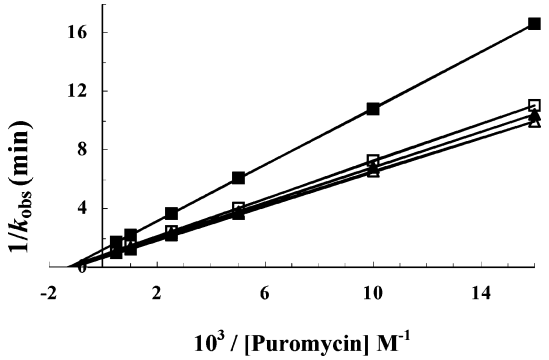

FIGURE 5: Peptidyltransferase activity of the *rdn* mutant ribosomes. From the double reciprocal plots ($1/k_{obs}$ versus 1/[puromycin]), the values of k_3 and K_s for all strains were determined. The plots represent *rdnwt* (open triangles), *rdn1A* (solid squares), *rdn1T* (solid triangles), and *rdn2* (open squares).

Table 4: Proportion of Ribosomal Particles Isolated from Wild-Type or Mutant Cells following Sucrose Gradient Analysis

	strain			
ribosomal species	*rdnwt*	*rdn1A*	*rdn1T*	*rdn2*
polysomes and 80S monosomes (%)	86.7	86.2	86.4	86.6
60S subunits (%)	9.6	11.7	9.7	9.2
40S subunits (%)	3.7	2.1	3.9	4.2
60S/40S	2.6	5.6	2.5	2.2

Equation 2 predicts that a plot of the reciprocal of the experimental k_{obs} versus the reciprocal of the puromycin concentration (double reciprocal plot) should be linear. The values of k_{obs} obtained for the wild-type strain were fitted in eq 2 from which the double reciprocal plot gave $k_3 = 1.46$ min^{-1} and $K_s = 0.85$ mM (Table 3 and Figure 5).

The reaction of complex C from the *rdn* mutant strains with puromycin followed also pseudo-first-order kinetics, and the semilogarithmic time plots were also linear. Double reciprocal plots were linear, too (Figure 5). From these plots the first-order catalytic rate constants (k_3) for the *rdn1A*, *rdn1T*, and *rdn2* ribosomes were estimated at 0.82, 1.32, and 1.25 min^{-1}, respectively (Table 3). The dissociation constant K_s remained essentially the same for all mutants. Thus, ratio k_3/K_s, a second-order rate constant, which is an accurate measure of peptidyltransferase activity, was estimated at 1.04, 1.65, and 1.67 min^{-1} mM^{-1}, respectively, compared to 1.72 min^{-1} mM^{-1} for *rdnwt*. In conclusion, mutation C1054A (*rdn1A*) lowered peptidyltransferase activity to about half its normal value, whereas mutations C1054U and G517A caused no significant effect on the catalytic properties of the yeast ribosome.

Mutation rdn1A Causes an Imbalance in Ribosomal Subunits. From the polysome profiles of mutant and wild-type strains, a significant decrease in the proportion of 40S subunits in the error-prone strain carrying mutation *rdn1A* was observed (Table 4). This was accompanied by an increase in the proportion of 60S subunits. The ratio of 60S:40S was raised to 5.6 compared to 2.6 for the wild-type strain. This subunit imbalance may be responsible for the poor growth phenotype displayed by *rdn1A*. In contrast, mutation *rdn1T*, carrying uracil instead of adenine in position 1054, did not affect the amount of 40S or 60S subunits, and the ratio remained the same as for wild type, i.e., 60S:40S equal to 2.5. Mutation *rdn1T* did not influence the amount of 80S ribosomes or polysomes either. Equally, the polysome and ribosomal subunit profile of *rdn2*, the third mutation under study, was similar to that of *rdnwt*.

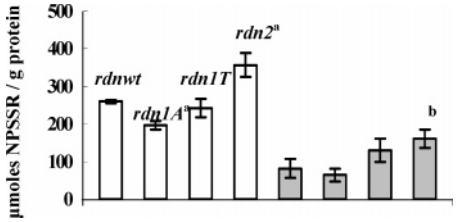

FIGURE 6: Nonprotein disulfide levels, expressed in micromoles of NPSSR per gram of protein, for *rdnwt* and *rdn* mutant strains in the absence (white panels) or in the presence (gray panels) of 150 μM paromomycin. The sequence of the paromomycin-treated strains is the same as when no paromomycin was used. Each value represents the mean ± SE of triplicate measurements of two independent experiments. Footnotes: a, statistically different (one-way analysis of variance, F-Scheffè test, $p < 0.05$) from the wild type in the absence of PM; b, statistically different (one-way analysis of variance, F-Scheffè test, $p < 0.05$) from the wild type in the presence of 150 μM PM.

Oxidative Stress Studies. It is known that translational fidelity and the oxidative balance are two among several parameters altered, as cells grow old (*27*). To examine if these translational fidelity mutations affect the oxidative balance of the cell, we grew all rRNA mutant strains until the late log phase where cell divisions are minimized, and we determined the levels of four oxidative stress markers, i.e., the nonprotein disulfides, the lipid peroxides, the protein thiols, and protein disulfides.

Nonprotein disulfides consist of molecules that carry sulfur atoms, which are joined together via disulfide bonds. As shown in Figure 6 (white panels), the error-prone mutation *rdn1A* exhibited the least pronounced oxidative modifications since the number of disulfide bonds formed between nonprotein thiol molecules was significantly decreased compared to *rdnwt* and the other strains. In contrast, the error-restrictive mutation *rdn2* formed more disulfide bonds between nonprotein thiol molecules, an indication of a higher level of oxidative modifications than wild type. The other error-restrictive mutation under study, *rdn1T*, displayed no significant difference compared to *rdnwt*.

A similar pattern was obtained when malondialdehyde (MDA) levels were determined. MDA is the product of lipid peroxidation and serves as a specific oxidative stress marker. The strongly error-prone mutation *rdn1A* and the strongly error-restrictive mutation *rdn2* caused a pronounced decrease and increase in MDA production, respectively (Figure 7, white panels). Mutation *rdn1T*, the second and less pronounced error-restrictive mutation, failed to show any significant change in the amount of MDA produced.

Two further redox state markers were determined in the present study, the reduced protein thiols (PSH) carrying sulfhydryl groups and the oxidized protein thiols (PSSP) carrying disulfide bridges. High levels of PSH and low levels of PSSP are two indicators of lower oxidative stress. Mutation *rdn1A* caused a 2-fold increase in the levels of PSH, whereas mutations *rdn1T* and *rdn2* caused a decrease in PSH levels to almost zero (Table 5). Moreover, the levels of PSSP were lowered in *rdn1A* and, conversely, increased in both error-restrictive mutations, with *rdn2*, the more error-restrictive of the two, showing the highest increase. Ratio PSH/PSSP is, therefore, a reliable index of the redox state

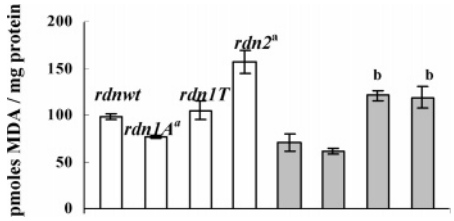

FIGURE 7: Lipid peroxidation levels, expressed in picomoles of malondialdehyde (MDA) per milligram of protein, for *rdnwt* and *rdn* mutant strains in the absence (white panels) or in the presence (gray panels) of 150 μM paromomycin. The sequence of the paromomycin-treated strains is the same as when no paromomycin was used. Each value represents the mean ± SE of triplicate measurements of two independent experiments. Footnotes: a, statistically different (one-way analysis of variance, F-Scheffè test, $p < 0.05$) from the wild type in the absence of PM; b, statistically different (one-way analysis of variance, F-Scheffè test, $p < 0.05$) from the wild type in the presence of 150 μM PM.

Table 5: Levels of Protein Thiols (PSH) and Protein Disulfides (PSSP) in Wild-Type and Mutant Yeast Cells

	strain			
redox marker	*rdnwt*	*rdn1A*	*rdn1T*	*rdn2*
PSH (μmol/g of protein)	12	26	4	~0
PSSP (μmol/g of protein)	107	71	164	199
PSH/PSSP	0.11	0.37	0.024	~0

of a cell. A 3-fold increase signifies lower oxidative stress for the error-prone mutant *rdn1A*, whereas a decrease to 0.024 and to 0 signifies higher oxidative stress for *rdn1T* and, especially, *rdn2*, respectively.

Effect of an Error-Inducing Antibiotic on Oxidative Stress. If the hypothesis is true that an error-prone cell causes less oxidative stress, then it is possible that an error-inducing antibiotic such as paromomycin also reduces oxidative stress. This hypothesis was tested in a similar series of experiments in which cells from the various strains were grown in the presence of paromomycin.

At 150 μM paromomycin an almost 2-fold decrease in the growth rates of all strains was observed, presumably due to impaired protein synthesis capacity. This error-inducing antibiotic caused a reduction of nonprotein disulfides (Figure 6, gray panels) and lipid peroxides (Figure 7, gray panels) in all strains, while retaining intact the character of each strain as defined in Figures 6 and 7 (white panels). Thus, in the presence of paromomycin, even *rdn1T*, which is only slightly hyperaccurate, showed a statistically significant increase in the amount of MDA produced compared with wild type. These results offer additional evidence that the loss of accuracy is associated with a decrease of oxidative stress, while hyperaccuracy is combined with an increase of oxidative stress.

DISCUSSION

In the present work we carried out a detailed biochemical analysis of the effect of yeast 18S rRNA mutations *rdn1A*, *rdn1T*, and *rdn2* (Figure 1) on several parameters of protein synthesis and on specific functions of the cell. Genetic studies had shown previously that these mutations interfere with translational termination and with changes in the resistance to paromomycin (*16*, *17*, *28*). We confirm that these mutations behave as translational suppressors or antisuppressors and provide in vitro evidence that yeast C1054 in helix 34 and G517 in helix 18 of 18S rRNA are in fact crucial for the control of general translational fidelity.

We show that mutation *rdn1A* in yeast (C1054A) increased significantly the error rate (Table 2), and this was accompanied by higher sensitivity toward paromomycin (Figure 4). These results confirm earlier findings that *rdn1A* caused translational suppression at stop codons (*16*) and show that *rdn1A* generates translational infidelity at sense codons as well. In contrast, *rdn1T* (C1054U) decreased the error rate, and this was accompanied by a slightly increased resistance to paromomycin. Apparently, different substitutions at the same position (C1054) may cause opposite effects, i.e., suppression and general translational infidelity or antisuppression and enhanced fidelity. The significance of C1054 was also drawn from the sucrose gradient analysis of polysomes of the *rdn1A* and *rdn1T* strains. Indeed, the polysome profile data suggest that the balance in ribosomal subunits is compromised by the C1054A substitution, while it remains intact by the C1054U substitution (Table 4). This difference may explain the poor growth of *rdn1A* mutants and the near normal growth of *rdn1T* mutants.

Furthermore, we show that the third mutation under study, *rdn2* (G517A), decreased the error rate to nearly zero, making it the most hyperaccurate mutation studied thus far. Such hyperaccuracy is even more interesting as the possibility of a mixed population of ribosomes cannot be entirely excluded. However, error rates near zero were repeatedly obtained from successive ribosomal preparations of this strain. A substantially higher resistance to paromomycin accompanied this hyperaccuracy.

Binding of cognate aminoacyl-tRNA to the A-site proceeds rapidly and efficiently with essentially no rejection. In contrast, most of near-cognate aminoacyl-tRNA is rejected due to both low stability of aminoacyl-tRNA binding and lower rate of accommodation (*13*). The error-prone mutation *rdn1A* showed increased stability of cognate aminoacyl-tRNA binding while error-restrictive mutations *rdn1T* and *rdn2* showed decreased stability. Since A-site binding is a nonequilibrium process driven by the irreversible forward reactions of GTP hydrolysis and peptide bond formation (*29*), these differences in stability may be the result of conformational changes at the decoding center.

Further support for the importance of conformational changes at the decoding center comes from kinetic studies of the error-inducing effect of the antibiotic paromomycin (*29*, *30*) combined with the crystal structures of 30S subunits with cognate or near-cognate substrates stabilized by the antibiotic (*7*, *8*). Paromomycin causes the same conformational change at the decoding center even in the absence of correct codon−anticodon interaction. Formation of the complex stabilizes near-cognate aminoacyl-tRNA and increases the rate of GTP hydrolysis in the near-cognate ternary complex almost to the level of the cognate substrate (*13*).

In *E. coli*, substitutions C1054A and G517A behaved as translational suppressors and reduced translational fidelity, whereas substitution C1054U did not cause either suppression or antisuppression (*18*, *19*, *31*). Moreover, mutant ribosomes from *E. coli* carrying a deletion in this position, C1054Δ, caused suppression of all three nonsense codons, pointing to a possible effect of C1054 on translational termination (*32*). Thus, it is quite interesting that, of the three translational fidelity mutations under study, only one, *rdn1A* (C1054A),

maintained the same direction in yeast as in *E. coli*. Mutation *rdn1T* (C1054U) caused hyperaccuracy in yeast versus no suppression or even antisuppression in *E. coli*, while mutation *rdn2* (G517A) caused extreme hyperaccuracy in yeast versus suppression in *E. coli*.

The rate of peptide bond formation was measured by the puromycin reaction, a pseudo-first-order reaction. At saturating concentrations of puromycin, the catalytic rate constant k_3 is independent of the puromycin concentration and of the population of active ribosomes. Therefore, k_3 would be the same regardless of whether the percentage of active ribosomes was higher or lower than the 10.6% reported here. Mutation *rdn1A* reduced the rate of peptide bond formation to half its normal value (Table 3 and Figure 5), not quite sufficient to make it essential for peptide bond formation but enough to make this region of 18S rRNA a contributory factor for ribosome's optimal catalytic activity, possibly via allosteric interactions. The catalytic center of a ribosome may be composed entirely from specific nucleotides of the large ribosomal subunit rRNA (*4*), but the fine-tuning of this activity involves in addition a number of elements of both subunits. In *E. coli*, ribosomal protein L2 of the 50S subunit was shown to be involved in ribosomal association, in tRNA binding to A- and P-sites, and in peptidyl transfer (*33*). In yeast, these elements include ribosomal proteins L24 (*34*) and L41 (*35*) of the 60S subunit as well as a number of nucleotides, such as C2658 of 25S rRNA (*14*) and, as shown here, C1054 of 18S rRNA.

The fact that mutation *rdn1A* transcends the confines of the small ribosomal subunit and has an impact on the catalytic activity of the ribosome, an activity associated with the large ribosomal subunit, is one more indication that the two ribosomal subunits are in constant intercommunication. In agreement with this notion, the absence of ribosomal protein L39 of the 60S subunit decreases the fidelity of translation (*15*), and mutation C2658U of 25S rRNA, in addition to its fine-tuning of ribosomal catalytic activity, decreases also the fidelity of translation (*14*). Interaction between the distant decoding and catalytic sites can be achieved either via transmission of conformational changes within and between the subunits or via ribosome-associated factors or substrates connecting the different sites. Both principles operate during protein synthesis (*36*).

The rate of polyphenylalanine synthesis was doubled in *rdn1A* mutants compared to wild type (Figure 3). Since A-site binding is the rate-limiting step of the elongation cycle of protein synthesis (*37*), a similar increase (75%) of A-site binding in *rdn1A* mutants may explain the increase in polyphenylalanine synthesis. Likewise, rates of polyphenylalanine synthesis for the *rdn1T* and *rdn2* strains similar to wild type reflect the lack of a sizable effect of these two mutations on A-site binding.

The fact that the rate of peptide bond formation of *rdn1A* mutants was reduced while the rate of polyphenylalanine synthesis was increased is explained by the assumption that these two processes have different rate-limiting steps. The rate-limiting step of the elongation cycle is the occupation of the A-site, and this is much slower than peptide bond formation (*37*, *38*). For the puromycin reaction, in contrast, the rate-limiting step is the formation of peptide bond and not the binding of puromycin to the A-site (*33*). As a result, a significant reduction in peptidyltransferase activity may strongly decrease the rate of puromycin reaction, and this may be independent from the rate of polyphenylalanine synthesis.

Finally, another major conclusion with far-reaching implications may be drawn from the present study. The changes in translational fidelity of the mutations under study affected the oxidative balance of the cell. Thus, the error-prone mutation *rdn1A* decreased lipid peroxidation and nonprotein/protein disulfides, factors that are indicators of high oxidative stress (Figures 6 and 7, Table 5). Additionally, protein thiols, an indicator of low oxidative stress, were increased. In the case of the nonprotein disulfides, free radicals can attack free thiols and convert them to thiol radicals, which in turn combine to form disulfides. Moreover, protein thiols and protein disulfides are important indicators of oxidative stress, since they can result (a) from formation of interdisulfide bridges between protein thiols (inter-PSSPs), leading to the formation of protein aggregates, and (b) from formation of intradisulfide bridges within proteins (intra-PSSPs) undergoing oxidative tertiary structure modification. Intraprotein disulfides are important thiol redox indicators as they are formed during the activation/inactivation of receptors, in the inactivation of enzymes, transporters, and transcriptional factors under conditions of oxidative stress, whereas interprotein disulfides are formed in animal cells during pathological processes associated with oxidative stress (*22*). In contrast to *rdn1A*, error-restrictive mutations *rdn1T* and *rdn2* increased oxidative stress, as indicated by the increased level of lipid peroxides and nonprotein and protein disulfides. Further comparison between *rdn1T* and *rdn2* revealed that *rdn2*, the more error-restrictive of the two, was also the mutation most susceptible to these oxidative modifications. Additional support for the hypothesis that error-prone cells exhibit less oxidative stress came from studies with paromomycin. This error-inducing antibiotic decreased both lipid peroxidation and the nonprotein disulfides.

The task of pinpointing the causal factors behind the increased oxidation modifications has proved to be difficult (*39*). Thus, Ballesteros et al. (*27*) have reported that carbonylation of proteins, another indicator of oxidative stress, was drastically attenuated in mutants with hyperaccurate ribosomes, whereas it was enhanced in mutants with error-prone ribosomes. However, it is possible that protein oxidation is the result of an increased rate of translation rather than an increased rate of error frequency (*20*).

A plausible explanation for our results is that the more hyperaccurate the cell, the higher the amount of energy it must spend, e.g. in the form of GTP, to achieve and maintain error-free protein synthesis to such a degree that it neglects other processes such as the elimination of free radicals. In contrast, error-prone cells have more energy available with which to combat free radicals. The present analysis is the first attempt to correlate translational infidelity with decreased oxidative stress in a eukaryotic microorganism.

ACKNOWLEDGMENT

We are indebted to Professor Susan Liebman for making yeast strains *rdn1A*, *rdn1T*, and *rdn2* available to us. We thank Professor Dimitrios Kalpaxis and Dr. John Dresios for critical reading of the manuscript.

REFERENCES

1. Schluenzen, F., Tocilj, A., Zarivach, R., Harms, J., Gluehmann, M., Janell, D., Bashan, A., Bartels, H., Agmon, I., Franceschi, F., and Yonath, A. (2000) Structure of functionally activated small ribosomal subunit at 3.3 angstroms resolution, *Cell 102*, 615−623.
2. Alksne, L. E., Anthony, R. A., Liebman, S. W., and Warner, J. R. (1993) An accuracy centre in the ribosome conserved over 2 billion years, *Proc. Natl. Acad. Sci. U.S.A. 90*, 9538−9541.
3. Nissen, P., Hansen, J., Ban, N., Moore, P. B., and Steitz, T. A. (2000) The structural basis of ribosome activity in peptide bond synthesis, *Science 289*, 920−930.
4. Noller, H. F. (2005) RNA structure: Reading the ribosome, *Science 309*, 1508−1514.
5. Spahn, C. M., Beckmann, R., Eswar, N., Penczek, P. A., Sali, A., Blobel, G., and Frank, J. (2001) Structure of the 80S ribosome from *Saccharomyces cerevisiae*−tRNA-ribosome and subunit-subunit interactions, *Cell 107*, 373−386.
6. Yoshizawa, S., Fourmy, D., and Puglisi, J. D. (1999) Recognition of the codon-anticodon helix by ribosomal RNA, *Science 285*, 1722−1725.
7. Ogle, J., Brodersen, D. E., Clemons, W. M., Jr., Tarry, M. J., Carter, A. P., and Ramakrishnan, V. (2001) Recognition of cognate transfer RNA by the 30S ribosomal subunit, *Science 292*, 897−902.
8. Ogle, J. M., and Ramakrishnan, V. (2005) Structural insights into translational fidelity, *Annu. Rev. Biochem. 74*, 129−177.
9. Carter, A. P., Clemons, W. M., Brodersen, D. E., Morgan-Warren, R. J., Wimberly, B. T., and Ramakrishnan, V. (2000) Functional insights from the structure of the 30S ribosomal subunit and its interactions with antibiotics, *Nature 407*, 340−348.
10. Belanger, F., Gagnon, M. G., Steinberg, S. V., Cunnigham, P. R., and Brakier-Gingras, L. (2004) Study of the functional interaction of the 900 tetraloop of 16S ribosomal RNA with helix 24 within the bacterial ribosome, *J. Mol. Biol. 338*, 683−693.
11. Yusupov, M. M., Yusupova, G. Z., Baucom, A., Lieberman, K., Earnest, T. N., Cate, J. H., and Noller, H. F. (2001) Crystal structure of the ribosome at 5.5 Å resolution, *Science 292*, 883−896.
12. O'Connor, M., Thomas, C. L., Zimmermann, R. A., and Dahlberg, A. E. (1997) Decoding fidelity at the ribosomal A and P sites: influence of mutations in three different regions of the decoding domain in 16S rRNA, *Nucleic Acids Res. 25*, 1185−1193.
13. Rodnina, M. V., Gromadski, K. B., Kothe, U., and Wieden, H. J. (2005) Recognition and selection of tRNA in translation, *FEBS Lett. 579*, 938−942.
14. Panopoulos, P., Dresios, J., and Synetos, D. (2004) Biochemical evidence of translational infidelity and decreased peptidyltransferase activity by a sarcin/ricin domain mutation of yeast 25S rRNA, *Nucleic Acids Res. 32*, 5398−5408.
15. Dresios, J., Derkatch, I. L., Liebman, S. W., and Synetos, D. (2000) Yeast ribosomal protein L24 affects the kinetics of protein synthesis and ribosomal protein L39 improves translational accuracy, while mutants lacking both remain viable, *Biochemistry 39*, 7236−7244.
16. Chernoff, Y. O., Newnam, G. P., and Liebman, S. W. (1996) The translational function of nucleotide C1054 in the small subunit rRNA is conserved throughout evolution: genetic evidence in yeast, *Proc. Natl. Acad. Sci. U.S.A. 93*, 2517−2522.
17. Chernoff, Y. O., Vincent, A., and Liebman, S. W. (1994) Mutations in eukaryotic 18S ribosomal RNA affect translational fidelity and resistance to aminoglycoside antibiotics, *EMBO J. 13*, 906−913.
18. O'Connor, M., Goringer, H. U., and Dahlberg, A. E. (1992) A ribosomal ambiguity mutation in the 530 loop of *E. coli* 16S rRNA, *Nucleic Acids Res. 20*, 4221−4227.
19. Murgola, E. J., Hijazi, K. A., Goringer, H. U., and Dahlberg, A. E. (1988) Mutant 16S ribosomal RNA: a codon specific translational suppressor, *Proc. Natl. Acad. Sci. U.S.A. 85*, 4162−4165.
20. Dukan, S., and Nyström, T. (1998) Bacterial senescence: stasis results in increased and differential oxidation of cytoplasmic proteins leading to developmental induction of the heat shock regulon, *Genes Dev. 12*, 3431−3441.
21. Dukan, S., Farewell, A., Ballesteros, M., Taddei, F., Radman, M., and Nyström, T. (2000) Protein oxidation in response to increased transcriptional or translational errors, *Proc. Natl. Acad. Sci. U.S.A. 97*, 5746−5749.
22. Patsoukis, N., and Georgiou, C. D. (2004) Determination of the thiol redox state of organisms: new oxidative stress indicators, *Anal. Bioanal. Chem. 378*, 1783−1792.
23. Cundliffe, E. (1990) in *The Ribosome: Structure, Function and Evolution* (Hill, W. E., Dahlberg, A. E., Garrett, R. A., Moore, P. B., Schlessinger, D., and Warvew, J. R., Eds.) pp 579−590, American Society of Microbiology, Washington, DC.
24. Fourmy, D., Yoshizawa, S., and Puglisi, J. D. (1998) Paromomycin binding induces a local conformational change in the A-site of 16 S rRNA, *J. Mol. Biol. 277*, 333−345.
25. Liu, R., and Liebman, S. W. (1996) A translational fidelity mutation in the universally conserved sarcin/ricin domain of 25S yeast ribosomal RNA, *RNA 2*, 254−263.
26. Velichutina, I. V., Dresios, J., Hong, J. Y., Li, C., Mankin, A., Synetos, D., and Liebman, S. W. (2000) Mutations in helix 27 of the yeast *Saccharomyces cerevisiae* 18S rRNA affect the function of the decoding center of the ribosome, *RNA 6*, 1174−1184.
27. Ballesteros, M., Fredriksson, A., Henriksson, J., and Nyström, T. (2001) Bacterial senescence: protein oxidation in non-proliferating cells is dictated by the accuracy of the ribosomes, *EMBO J. 20*, 5280−5289.
28. Liebman, S. W., Chernoff, Y. O., and Liu, R. (1995) The accuracy centre of a eukaryotic ribosome, *Biochem. Cell Biol. 73*, 1141−1149.
29. Gromadski, K. B., and Rodnina, M. V. (2004) Streptomycin interferes with conformational coupling between codon recognition and GTPase activation on the ribosome, *Nat. Struct. Mol. Biol. 11*, 316−322.
30. Pape, T., Wintermeyer, W., and Rodnina, M. V. (2000) Conformational switch in the decoding region of 16S rRNA during aminoacyl-tRNA selection on the ribosome, *Nat. Struct. Biol. 7*, 104−107.
31. Murgola, E. J., Pagel, F. T., Hijazi, K. A., Arkov, A. L., Xu, W., and Zhao, S. Q. (1995) Variety of nonsense suppressor phenotypes associated with mutational changes at conserved sites in *Escherichia coli* ribosomal RNA, *Biochem. Cell Biol. 73*, 925−931.
32. Prescott, C., Krabben, L., and Nierhaus, K. (1991) Ribosomes containing the C1054-deletion mutation in *E. coli* 16S rRNA act as suppressors at all three nonsense codons, *Nucleic Acids Res. 19*, 5281−5283.
33. Diedrich, G., Spahn, C. M. T., Stelzl, U., Schäfer, M. A., Wooten, T., Bockhariov, D. E., Cooperman, B. S., Traut, R. R., and Nierhaus, K. H. (2000) Ribosomal protein L2 is involved in the association of the ribosomal subunits, tRNA binding to A and P sites and peptidyl transfer, *EMBO J. 19*, 5241−5250.
34. Dresios, J., Panopoulos, P., Frantziou, C. P., and Synetos, D. (2001) Yeast ribosomal protein deletion mutants possess altered peptidyltransferase activity and different sensitivity to cycloheximide, *Biochemistry 40*, 8101−8108.
35. Dresios, J., Panopoulos, P., Suzuki, K., and Synetos, D. (2003) A dispensable yeast ribosomal protein optimizes peptidyltransferase activity and affects translocation, *J. Biol. Chem. 278*, 3314−3322.
36. Rospert, S. (2004) Ribosome function: governing the fate of a nascent polypeptide, *Curr. Biol. 14*, 386−388.
37. Schilling-Bartetzko, S., Bartetzko, A., and Nierhaus, K. H. (1992)-Kinetic and thermodynamic parameters for tRNA binding to the ribosome and for the translocation reaction, *J. Biol. Chem. 267*, 4703−4712.
38. Bilgin, N., Kirsebom, L. A., Ehrenberg, M., and Kurland, C. G. (1988) Mutations in ribosomal proteins L7/L12 perturb EF-G and EF-Tu functions, *Biochimie 70*, 611−618.
39. Sohal, R. S., Agarwal, S., and Sohal, B. H. (1995) Oxidative stress and aging in the Mongolian gerbil (*Meriones unguiculatus*), *Mech. Aging Dev. 81*, 15−25.

BI052505D